Medical Engineering and Physics 73 (2019) 18–29

Contents lists available at ScienceDirect

Medical Engineering and Physics

journal homepage: www.elsevier.com/locate/medengphy

Characterising the mechanical properties of haematopoietic and mesenchymal stem cells using micromanipulation and atomic force microscopy

Mingming Du[a], Dean Kavanagh[b], Neena Kalia[b,*], Zhibing Zhang[a,*]

[a] School of Chemical Engineering, University of Birmingham, Birmingham B15 2TT, UK
[b] Institute of Cardiovascular Sciences, University of Birmingham, Birmingham B15 2TT, UK

ARTICLE INFO

Article history:
Received 19 August 2018
Revised 12 July 2019
Accepted 21 July 2019

Keywords:
Haematopoietic stem cells
Mesenchymal stem cells
Deformability
Micromanipulation
Atomic force microscopy
Young's modulus

ABSTRACT

Background: Improving stem cell (SC) deformability using pre-treatment strategies, or isolating more deformable sub-populations, may prevent non-specific entrapment of injected cells, maintain circulating numbers and thus increase the likelihood of capture by microvessels in injured organs. However, nothing is currently known about the basic mechanical properties of SCs, particularly with regards their elastic characteristics. This study therefore aimed to determine the mechanical characteristics of haematopoietic stem cells (HSCs) and mesenchymal stem cells (MSCs) with comparisons made to neutrophils.
Methods: Micromanipulation and atomic force microscopy (AFM) were used to quantitate mechanical properties following large and small deformations respectively of neutrophils, MSCs and naïve and stromal cell-derived factor-1α (SDF-1α) or hydrogen peroxide (H_2O_2) pre-treated HSCs.
Results: Neutrophils and HSCs underwent rupture at ~80% deformation. Nominal rupture stress (σ_R), nominal rupture tension (T_R) and the Young's/elastic modulus at large deformations was significantly higher for neutrophils indicating they were stiffer and less deformable than HSCs. Surprisingly, MSCs did not rupture and were as deformable as HSCs despite their large size. Pre-treatment increased HSC deformability as indicated by lower rupture force, σ_R, T_R and Young's modulus at large deformations. AFM demonstrated that pre-treatment increased the Young's modulus at smaller deformations indicating the HSC surface stiffened. This was accompanied by increased F-actin accumulation and its localisation in the cell cortex.
Conclusion: This is the first study to precisely demonstrate that mechanical distinctions exist amongst different therapeutic SCs with regards their deformability and rupture response to applied stress. This can potentially be utilized as label-free markers in microfluidic cell sorting systems to separate sub-populations of potentially more therapeutic SCs.

1. Introduction

Haematopoietic (HSCs) and mesenchymal (MSCs) stem cells (SCs) are considered the leading cells for treating a whole host of inflammatory and degenerative diseases [1–6]. Novel bioengineering strategies have been applied to generate HSCs and MSCs with enhanced proliferative and differentiative capabilities, and a better ability to survive oxidative stress, a condition common to many diseases [7–10]. Both cell types confer therapeutic benefit through paracrine release of anti-apoptotic, anti-inflammatory, immunomodulatory and/or trophic growth factors. Recent studies have indicated that direct transplantation of SCs, protected within encapsulation systems such as hydrogels, is one mode of delivery [11,12]. However, clinically, the preferred and safest route of delivery of exogenous HSCs / MSCs is direct infusion into the bloodstream as this is both non-invasive and permits repeated injection of cells [6,13]. Systemic delivery relies on the capture of circulating SCs by the injury site microvasculature. This is an essential prerequisite event for successful therapy regardless of the reparative mechanism by which SCs confer benefit. However, local SC-endothelial interactions, and thus tissue recruitment, is poor and this has significantly impacted the clinical success of cellular therapy.

A major contributor to poor recruitment is the limited availability of circulating SCs in the peripheral blood post-infusion due to their non-specific entrapment within microvessels of non-diseased or non-injured organs. Both SC types cause considerable vascular obstructions following systemic injection primarily within

* Corresponding authors.
E-mail addresses: n.kalia@bham.ac.uk (N. Kalia), z.zhang@bham.ac.uk (Z. Zhang).

https://doi.org/10.1016/j.medengphy.2019.07.013
1350-4533/

pulmonary capillaries. This is a particular problem for MSCs which are a larger cell type compared to HSCs [14–16]. In addition to size, poor SC deformability may also contribute to their inability to pass through pulmonary capillaries. The importance of mechanical deformation in preventing cellular microvascular entrapment is highlighted by the fact that it is a key player in permitting neutrophils, with diameters of 6–8 µm, to traverse smaller pulmonary capillaries, with diameters of 2–15 µm [17,18]. In their transit through pulmonary and systemic microcirculations, neutrophils undergo a significant deformation when subjected to mechanical stimulation in narrow capillaries [19]. This ability to avoid entrapment allows neutrophils to typically be the first leukocyte to be recruited to an inflammatory site where they aid in the elimination of pathogens.

This suggests that strategies that can modify the deformability of injected SCs may potentially limit their physical entrapment within pulmonary capillaries and thus maintain their presence within the circulation [15,20]. This would increase the likelihood of their capture by microvessels at sites of injury and thus impact positively on their therapeutic efficacy. Indeed, we have previously shown using a basic micropipette aspiration methodology that pre-treatment of murine HSCs with soluble inflammatory factors, such as stromal cell-derived factor-1α (SDF-1α), significantly improved their deformability [21]. Intravital microscopy showed that this consequently enhanced the number of circulating HSCs passing through the peritubular capillaries of ischaemically injured kidneys. This was in comparison to control cells which only demonstrated a single pass immediately after infusion. Importantly, the continual re-circulation of HSCs, due to fewer cells being lost to non-specific entrapment within extra-renal sites, resulted in enhanced adhesion within the injured kidney.

An alternative strategy involves the specific isolation of deformable cells from a population of SCs prior to their infusion. Decreased cell deformability due to the cytoskeleton changing from a rigid structure to a more irregular and compliant state is a well established phenomenon assaociated with the malignant transformation of cells [22,23]. Indeed, this phenomenon could be exploited for diagnostic purposes with high throughput devices such as microfluidic optical stretchers [24]. Recently, label-free passive microfluidic systems for cell sorting have also been developed and are based on using the intrinsic biophysical markers of the cell, such as deformability, to separate them [25,26]. However, before we can utilize such systems to separate SCs for clinically therapeutic purposes, a more precise study of their biomechanical properties is needed. Currently, nothing is known about the basic mechanical properties of HSCs and MSCs, particularly with regards their elastic characteristics. Indeed it is not known whether both cell types possess similar deformability or whether there is heterogeneity within each population. Although we assume homogeneous mechanical properties within a single SC type, heterogeneity has been observed in many single cell populations.

Therefore, to characterise SC mechanical properties precisely, in the current study micromanipulation and atomic force microscopy (AFM) were utilised to apply forces to the whole cell (large deformation) or just the plasma membrane (small deformation) respectively. While techniques such as AFM have also been used as a tool to assess the mechanical properties of cancerous cells [27], the current study is the first to derive various mechanical property parameters for both HSCs and MSCs, including percentage deformation at rupture, force required to rupture the cell, nominal rupture stress and tension and also the Young's or elastic modulus of the cell. For HSCs, the effects of pre-treatment with soluble inflammatory factors on their mechanical behaviour was also determined. Polymerization of F-actin after pre-treatment was also assessed using flow cytometry and confocal microscopy.

2. Materials and methods

2.1. Culture of the murine HSC cell line, HPC-7

HPC-7 is functionally relevant murine hematopoietic progenitor cell line generated and immortalised by transfection of LIM-homeobox gene, Lhx2 into murine embryonic SCs. This cell line displays the critical characteristics of pure primary HSCs, such as being highly enriched for surface markers characteristic of the most immature HSCs (c-kit$^+$, Sca-1$^+$, CD34$^-$, Lin$^-$) [28,29]. We have further characterised the HPC-7 surface adhesion molecule profile and found it to be similar to primary HSCs [26–28]. We have also utilized HPC-7 s to investigate intravitally the mechanisms of HSC recruitment within injured kidney, gut and liver [21,30–32]. Therefore, the immortalized HPC-7 cell line was also used in this study. HPC-7 s were cultured in Stem Pro-34 SFM media (Life Technologies, Paisley, UK), 100 ng/mL stem cell factor (SCF, Life Technologies), 2 mM L-Glutamine (PAA, Somerset, UK), 50 U/mL penicillin and 50 U/mL streptomycin (PAA, Somerset, UK). Cells were counted daily and maintained at a density of between $0.8–1.3 \times 10^6$ cells/mL with medium replaced every two days. For some studies, 1×10^6 HSCs were pre-treated with either SDF-1α (10 ng/mL in 1 mL phosphate buffered saline - PBS; Peprotech, UK), hydrogen peroxide (H_2O_2 100 µM in PBS; Sigma-Aldrich, Poole, UK) or PBS vehicle for 30 mins at 37 °C. After pre-treatment, cells were washed, re-suspended in PBS and mechanically tested within 2 h.

2.2. Culture of murine bone marrow-derived MSCs

Bone marrow (BM)-derived MSCs were isolated from the fibulae and tibiae of fibulas of 8–12 week adult male C57BL/6 mice as previously described [14,33]. MSCs were cultured in a 6-well plate and maintained in minimum essential medium eagle-α supplemented with 10% fetal bovine serum (Sigma-Aldrich), L-glutamine (PAA Laboratories, Yeovil, UK), penicillin/streptomycin and 10 ng/mL transforming growth factor-β (New England Biolabs, Herts, UK). Cells between passage 4 and 9 were used for experiments and recovered by incubating them for 5 min at 37 °C with 0.25% trypsin/ethylenediaminetetraacetic acid (EDTA) solution. Immediately after trypsinization, cells were collected with a pipette, transferred to a 15 mL conical tube and centrifuged at 300x g for 5 min. Cells were re-suspended in PBS for mechanical testing.

2.3. Isolation of murine neutrophils

The density gradient separation method was used to isolate murine neutrophils from BM as previously described [34]. Briefly, rear legs were removed from 8–12 week adult male C57BL/6 mice and the BM was aspirated into a syringe. This cell suspension was filtered, washed and centrifuged and cells re-suspended in 2 mL EDTA (Sigma-Aldrich, Poole, UK). A Percoll gradient (2.5 mL 72%, 2.5 mL 64%, 2.5 mL 52%; Sigma-Aldrich, Poole, UK) was set up in a 15 mL falcon tube into which the cell suspension was added. The gradient was spun at 1500x g for 3 mins to separate the neutrophils from a fuzzy band of cells seen at the interface of the 72% and 64% Percoll. Collected neutrophils were washed and re-suspended in 1 mL PBS for mechanical testing.

2.4. Micromanipulation and atomic force microscopy

Micromanipulation involved compressing single cells suspended in medium between two parallel flat surfaces, namely the bottom of a glass chamber and a borosilicate 25 µM diameter glass probe [35,36]. The probe was driven downwards by a stepping motor at a speed of 2 µm/s until the cell ruptured and the probe made contact with the chamber. Since the probe was connected

to a force transducer (406A-ER, Aurora Scientific Inc. Canada) the force applied to each cell could be simultaneously obtained. From this measurement, a 'force versus displacement' graph was generated and used for calculation of additional mechanical parameters [35,36]. At least 20 randomly selected HSCs (naïve and pre-treated), MSCs and neutrophils were compressed to large deformations. Before compression, the cell diameter was directly measured from its image on the screen of an attached TV monitor.

HSCs were also mechanically tested following smaller deformations using a more sensitive AFM system with nanometer resolution which was operated in force-mapping mode (JPK NanoWizard^{R}). A silicon nitride cantilever with a 4 μm tip was used to probe the surface of the cell. Laser-tracking of the deflection of the cantilever probe was used to measure forces acting between the tip and the cell surface at a specific point which were recorded as a 'force versus height' curve. The cantilever tip was repeatedly advanced in the lateral direction to generate force curves from all compressed points. To prevent lateral movement of the spherical cells as they were probed, HSCs were immobilised onto a polystyrene surface coated with Cell-Tak solution (Corning, USA). A force profile was recorded and typical extend and retract curves were generated. A total area of 100 × 100 μm (64 × 64 pixels) was scanned. All immobilized cells in this area as well as the substrate surface were scanned and over four thousands force curves, which represented the compression of the cells or the substrate surface, were acquired. Data from at least 20 cells in each group was collected.

2.5. Determination of the Young's modulus from 'force versus displacement' data

The Young's modulus is a parameter calculated to represent the stiffness of the elastic material or cell being studied. Theoretically, the Hertz contact model may be valid and is commonly used to describe the relationship between the imposed force and displacement for small deformations of an elastic object. It has been successfully applied to yield the Young's modulus of different particles including cells when compressed to a small deformation [37–39]. In micromanipulation data processing, the Hertz contact model was also applied to calculate the Young's modulus using Eq. (1), having presumed that the individual cells were homogeneous, incompressible, spherical, elastic and there was no friction at the cell-substrate interfaces.

$$F = \frac{E * \sqrt{2R_c}}{3\left(1-\upsilon^2\right)}\delta^{3/2} \tag{1}$$

where F is the applied force, E is the Young's modulus of the cell, R_c is the original cell radius, υ is the Poisson's ratio of the cell (υ assumed to be 0.5 since cells are assumed to be incompressible material) and δ is the diametric compressive displacement. Higher values indicated cells that were less deformable for a given applied force and vice versa.

For calculation of the Young's modulus using data acquired by AFM, the Hertz model could only be used when probing a known geometry (spherical) over a flat surface [40]. Hence, selected force curves from the top, flat area of the cells were analyzed using Eq. (2) to fit the force data for calculation of the Young's modulus of the cell membrane [40].

$$F = \frac{4\sqrt{R_p}E}{3\left(1-\upsilon^2\right)}\delta^{3/2} \tag{2}$$

where R_p is the radius of the probe, and other parameters are the same as in Eq. (1).

2.6. Nominal rupture stress and nominal rupture tension

When compressed to a large deformation the cell may be ruptured and the corresponding rupture force determined. However, since the force required to rupture a cell depends on the initial size of the cell, it is difficult to compare the rupture force between different samples of cells if they have different sizes. Therefore, two additional parameters, which allowed meaningful comparisons of the mechanical strength of cells between different cell groups, were also quantitated. These parameters were nominal rupture stress (σ_R) and nominal rupture tension (T_R). Nominal rupture stress was defined by the ratio of the rupture force to the initial cross-sectional area as given by Eq. (3).

$$\sigma_R = \frac{4F_R}{\pi d^2} \tag{3}$$

where F_R is the rupture force and d is the original cell diameter before compression.

The nominal rupture tension was defined by the ratio of the rupture force and the original cell diameter, as shown in Eq. (4).

$$T_R = \frac{F_R}{d} \tag{4}$$

2.7. Analysis of F-actin with flow cytometry and confocal microscopy

PBS, SDF-1α or H_2O_2 pre-treated HSCs were fixed by incubating in 1 mL 2.5% formaldehyde for 10 mins. After washing in PBS, cells were permeabilised using 0.1% Triton-100 for 5–7 mins. Cells were blocked in PBS containing 5% normal fetal bovine serum and then labelled on ice with FITC-Phalloidin (Life Technologies, USA). At least 10,000 cells from each sample were analysed on a BD FACS Calibur cytometer (Becton Dickinson, USA) and data analysed with CellQuest (Becton Dickinson, USA). Such labelled cells were also imaged using confocal microscopy (Leica SP2; ×100 objective) microscopy. To reveal the localisation of F-action more clearly, multiphoton images of treated cells were also acquired. PBS, H_2O_2 and SDF-1α treated cells were again washed, fixed in 2.5% PFA, permeabilised with 0.1% Triton ×10 and resuspended in PBS containing 5% BSA to block non-specific binding for 30 mins on ice. Thereafter, cells were incubated with Alexa-555 Phallodin (1:500) and Hoescht 33,342 (10 ug/ml) for 45 mins on ice. Cells were mounted onto slides and imaged using an Olympus FV1000-MPE two-photon microscope using 800 nm and 1040 nm excitation wavelengths.

3. Results

3.1. Size of neutrophils, HSCs and MSCs

All types of SCs were larger in diameter when compared to neutrophils although MSCs were the largest type of cell (Table 1). The range of size was small for neutrophils (between 5 and 7 μm) but much larger for both HPC-7 s (6–13 μm) and MSCs (12–20 μm). There was no significant difference in the mean size or range of HSCs pre-treated with SDF-1α or H_2O_2 when compared to those pre-treated with the PBS control. SCs, particularly the larger MSCs, also demonstrated the relatively wider size span range, suggesting the smaller neutrophils were more homogeneous in their size distribution.

3.2. Neutrophils and HSCs share similarities in the force-displacement curves generated following large deformations

A typical relationship between the force imposed on the cell and the distance the probe travelled towards the chamber (displacement) for neutrophils and HSCs is shown (Fig. 1a,b). Despite their biological variation, common characteristics were observed in

Table 1
Pre-treatment with inflammatory factors does not change HSC size. The diameter of single cells was measured directly from the images captured using a camera attached to the micromanipulation rig. Neutrophils were the smallest in size compared to both stem cell types and MSCs were significantly bigger than HSCs. Stem cells showed greater variation or heterogeneity in their size distribution than neutrophils. Pre-treatment of HSCs with SDF-1α or H_2O_2 did not significantly affect their size. For each cell type, $n = 200$ individual cells that were measured. Data are presented as the means ± SEM.

Cell type	Mean (μm)	Size range (μm)
Neutrophils	6.6 ± 0.2	5–7
HPC-7s	10 ± 0.2	6–13
HPC-7s(SDF-1α)	10 ± 0.1	6–13
HPC-7s(H_2O_2)	10 ± 0.3	6–13
MSCs	16 ± 0.5	12–20

their compression curves. At point A, the probe started to touch the cell and force increased slowly with the displacement at fractional deformations of $\epsilon \sim 0.6$ (ϵ = displacement / initial cell diameter). From point B, in the region of $\epsilon \sim 0.6$–0.8, the force increased rapidly (region B-C) indicated by the increased gradient of the curve. This was followed by a force peak (point C) at which point the cell burst. Thereafter, the force decreased rapidly (to point D). Beyond 80% fractional deformation, the slope of the force curve increased more rapidly (region D-E).

Unlike neutrophils and HSCs, there was an absence of a peak force in the force-displacement curves of MSCs (Fig. 1c). In these cells, the force increased smoothly and slowly at low applied loads inducing fractional deformations of $\epsilon \sim 0$–0.8 of the cell membrane and cytoskeleton. The slope increased at ϵ >80% until the probe touched the bottom substrate where the slope of force curve increased more rapidly. The absence of a force peak demonstrated that there was no obvious rupture point or force for MSCs.

3.3. Nominal rupture stress / tension of HSCs at large deformations is less than neutrophils

The percentage deformation at rupture was not significantly different for neutrophils (75.3 ± 1.0%) and HSCs (79.3 ± 1.5%) with both rupturing when they were deformed to ~ 80% of their original size (Fig. 2a). The mean cell rupture force was also determined from the force-displacement curves (y-axis value at point C) for neutrophils (2.2 ± 0.3 μN) and HSCs (2.3 ± 0.2 μN) but was not significantly different between them (Fig. 2b). However, both nominal rupture stress σ_R ($p < 0.01$) and nominal rupture tension ($p < 0.01$) of HSCs was significantly less than neutrophils (Fig. 2c,d).

3.4. Young's modulus of HSCs & MSCs at large deformations is less than neutrophils

For each cell type, the elastic behaviour was still dominant up to a deformation of 60%. Hence the force-displacement data could be used to fit the Hertz equation for calculating the Young's elastic modulus at large deformations (data not shown). Fig. 2e illustrates the typical linear fitting based on the Hertz model to the experimental data for which a correlation coefficient of 0.9 was obtained. The calculated Young's modulus for neutrophils, HSCs and MSCs were 24.0 ± 1.8 kPa, 18.1 ± 0.3 kPa and 15.6 ± 1.2 kPa respectively with values for both HSCs ($p < 0.01$) and MSCs ($p < 0.01$) significantly lower than for neutrophils (Fig. 2f).

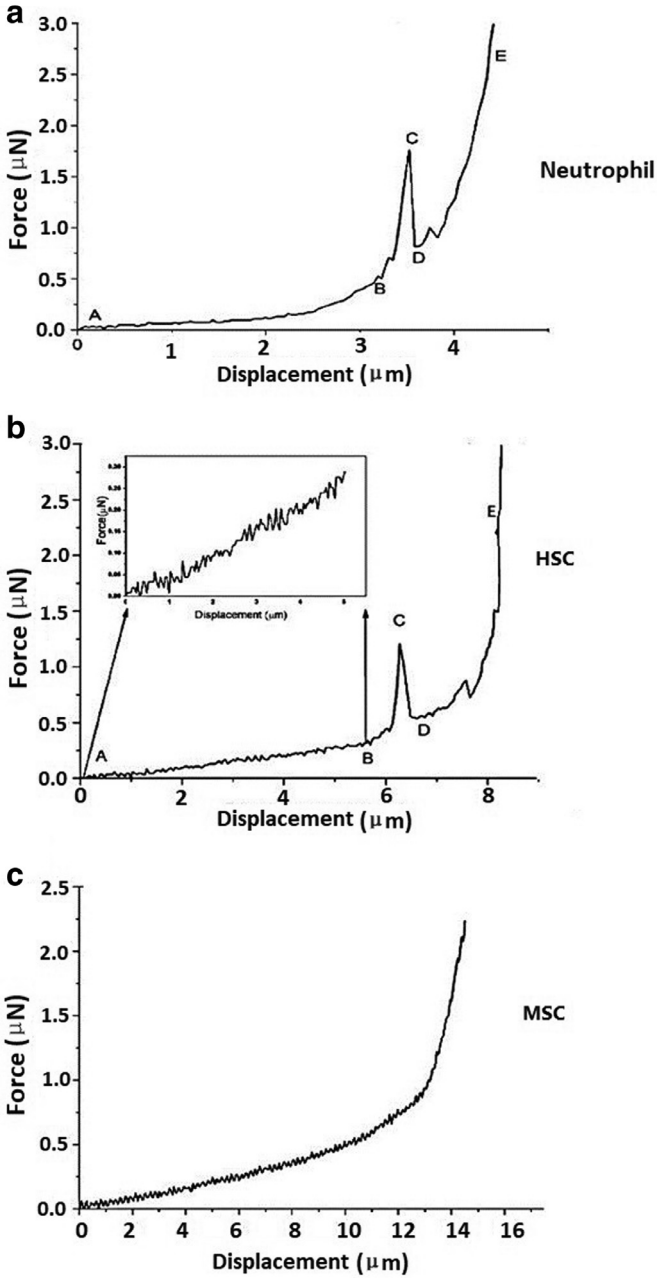

Fig. 1. *Neutrophils and HSCs share similarities in the force-displacement curves generated following large deformations during micromanipulation compression.* Typical force-displacement curves for **(a)** neutrophils and **(b)** HSCs show that force increases slowly with displacement as shown in region AB of the curve. As cells are further deformed, the gradient increases as shown in region BC of the curve. This is followed by the cell bursting at point C, with the force decreasing rapidly to point D, after which the force increases rapidly corresponding to the compression of cell debris and glass substrate as shown in region DE. **(c)** For MSCs, the force increases smoothly with displacement with no cells demonstrating a clear rupture point. All cells were compressed at a speed of 2 μm/s. $N = 20$ individual cells for each cell type.

3.5. Rupture force, nominal rupture stress / tension and Young's modulus of HSCs at large deformations decreases with SDF-1α and H_2O_2 pre-treatment

Pre-treatment did not affect rupture force with all HSCs still rupturing when they were deformed to ~80% of their original size (Fig. 3a). However, the force required to induce rupture significantly decreased from 2.2 ± 0.3 μN after pre-treatment with PBS to 1.3 ± 0.1 μN and 1.6 ± 0.2 μN after pre-treating with SDF-1α

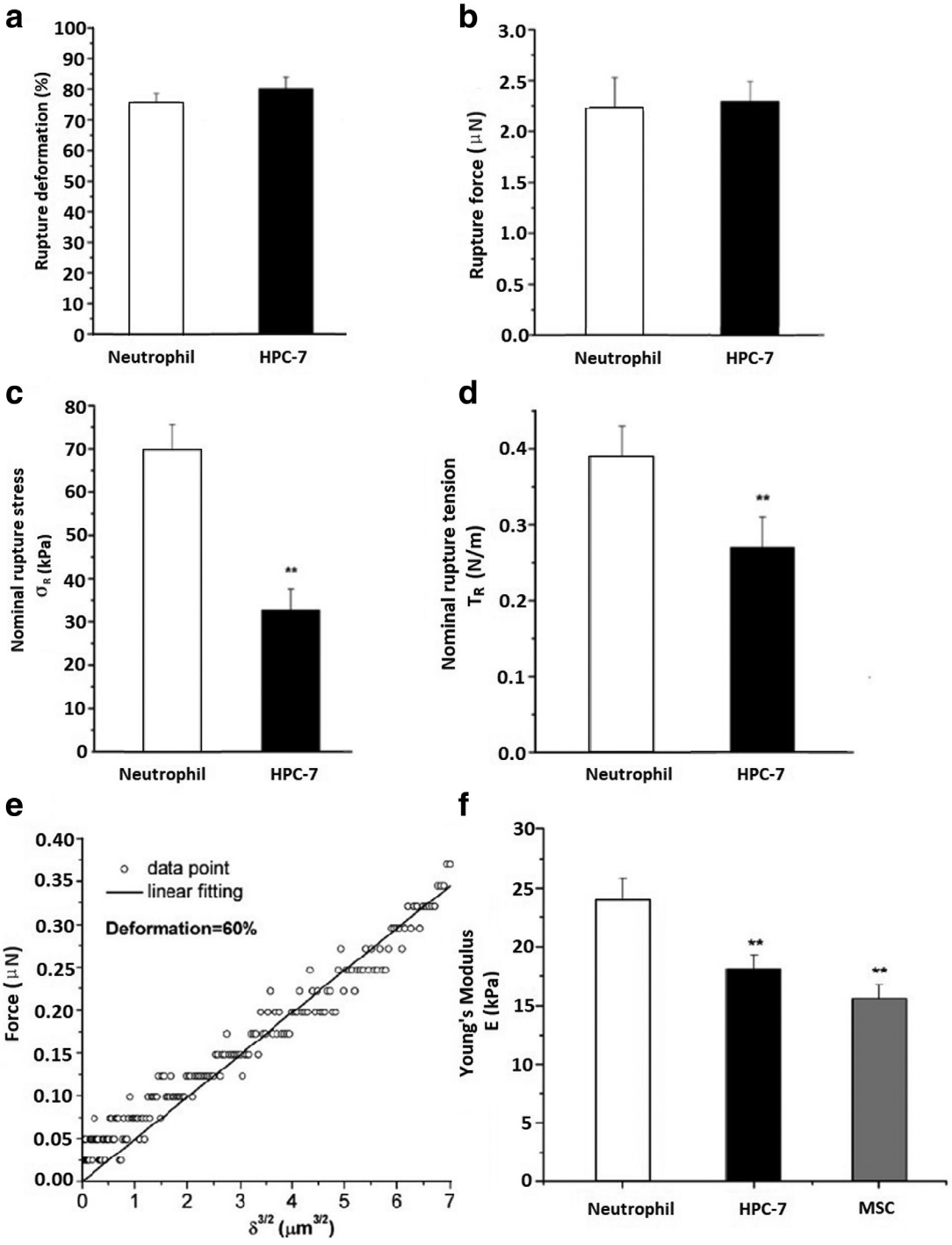

Fig. 2. *Nominal rupture stress and tension of HSCs and the Young's modulus of HSCs & MSCs at large deformations is less than neutrophils.* **(a)** Both neutrophils and HSCs were ruptured when their rupture deformation was close to 80%. **(b)** The forces required to rupture neutrophils and HSC were not significantly different. **(c)** Nominal rupture stress (σ_R) and **(d)** nominal rupture tension (T_R) of HSCs was significantly less than neutrophils indicative of neutrophils being stronger/stiffer cells with HSCs being 'weaker' cells. **(e)** Overall, the 'force versus displacement' curves obtained from the compression of all single cells up to a maximum deformation of 60% can be fitted to the Hertz model well. A typical straight line of the Hertz model was fitted to the force-displacement data (dot) obtained using micromanipulation with a correlation coefficient of 0.9. **(f)** Values of the Young's modulus for HSCs and MSCs were determined and shown to be less than neutrophils. Hence, although HSCs, and particularly MSCs, had larger cell sizes, they were less stiff and thus more deformable when compared to neutrophils. $N = 20$ individual cells for each group. Data is presented as mean ± SEM. $^{**}p < 0.01$ as determined using a paired student *t*-test.

($p < 0.01$) and H_2O_2 ($p < 0.01$) respectively (Fig. 3b). Both SDF-1α ($p < 0.01$) and H_2O_2 ($p < 0.01$) also significantly reduced the nominal rupture stress and tension (Fig. 3c,d). The Young's moduli of HSCs pre-treated with PBS, SDF-1α and H_2O_2 were 18.1 ± 1.2 kPa, 13.8 ± 0.8 kPa and 14.5 ± 0.8 kPa respectively with both SDF-1α ($p < 0.01$) and H_2O_2 ($p < 0.01$) pre-treated values being significantly lower than PBS treated cells (Fig. 3e).

3.6. Young's modulus of HSCs at small deformations increases with SDF-1α and H_2O_2 pre-treatment

AFM generated multicolour 3D surface topography images of individual HSCs, indicating the immobilization, intactness and spherical nature of scanned cells (Fig. 4a–d). Knowledge of the cell geometry was used to select force curves from a certain area on the

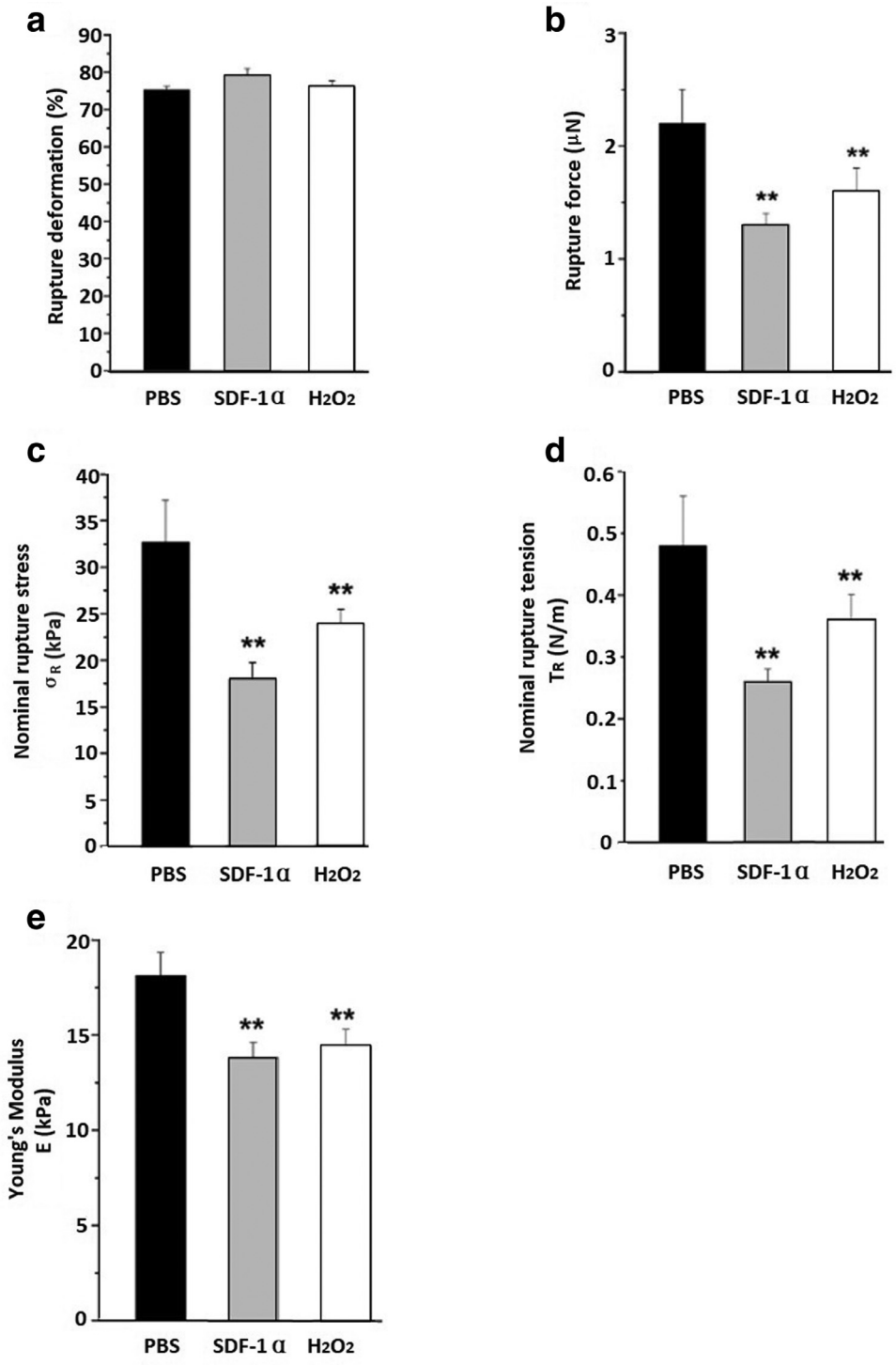

Fig. 3. *Rupture force, nominal rupture stress / tension and the Young's modulus of HSCs at large deformations decrease with SDF-1α and H_2O_2 pre-treatment.* **(a)** The mean rupture deformation for all of the pre-treatments was ~80%. **(b)** Forces required to rupture SDF-1α and H_2O_2 pre-treated HSCs were significantly smaller than that required to rupture PBS pre-treated cells. **(c)** Nominal rupture stress (σ_R) and **(d)** nominal rupture tension (T_R) of HSCs after pre-treating with SDF-1α and H_2O_2 significantly decreased. **(e)** A similar pattern of events was observed for the Young's modulus. Since a lower Young's modulus indicates more deformable cells, the data obtained at large deformations of 60% demonstrated that both pre-treatments generated HSCs which were significantly more deformable than PBS pre-treated cells. $N = 20$ individual cells for each group. Data is presented as mean ± SEM. $^{**}p < 0.01$ as determined using a paired Student *t*-test.

cell surface to determine their elastic modulus. The height information mapped to a colour value was used to distinguish single cells from the underlying substrate and was represented as a histogram showing the height distribution across the cross-section of a single cell (Fig. 4c). These histograms demonstrated that cells had some relatively flat areas, usually at their centre. This region met the condition of contact mode for calculation of the Young's modulus with the Hertz model [29]. To determine the elasticity for each cell, a collection of 'force versus displacement' curves were obtained at relatively flat areas from graphs showing the relationship between the piezo (z-height) movement and the cantilever deflection (Fig. 4e,f). The force-displacement data generated

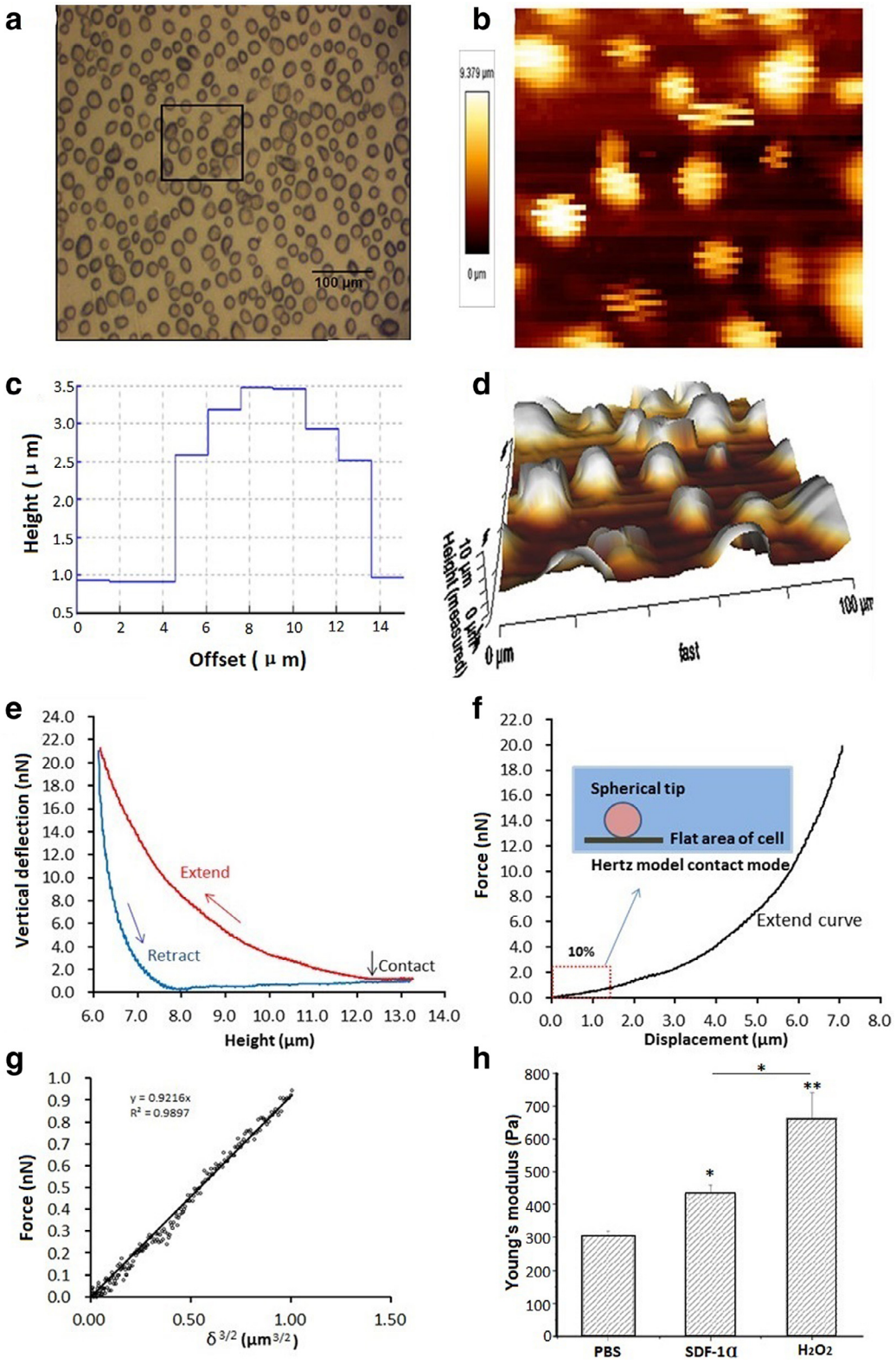

Fig. 4. *Topography information of HSCs and their Young's modulus at small deformations after SDF-1α and H_2O_2 pre-treatment using AFM.* **(a)** An image of the cell sample as observed through an optical microscope. The square box indicates an area of 100 × 100 µm that was analysed using AFM. Force scanning was conducted in this 100 × 100 µm area, a region equivalent to 64 × 64 pixels. **(b)** A typical 100 × 100 µm area is shown in which the height data was mapped to a colour value from which force curves were derived from the central area of the cell. The lightest colour represents the tallest part of the cells and the darkest colour represents the substrate. **(c)** 3D height projection showing the rough geometry of the cells in a 100 × 100 µm area. **(d)** Cross section of a single cell's height is shown based on plotting data with steps representing that the top points of the cell are relatively flat. **(e)** The force curves obtained by measurements of cantilever deflection versus height during extension and retraction of the probe. **(f)** The force-height curves were converted to force-displacement curves. The schematic illustrates compression of a spherical tip on the top area of the cell which was thought to be relatively flat. **(g)** The force-displacement curve, obtained at a deformation of less than 10% can be fitted to the Hertz model to calculate the Young's modulus. **(h)** The values of Young's modulus of the cell surface increased with SDF-1α or H_2O_2 indicative of increased cell surface stiffness after pre-treatment. $N = 3$ sets for each sample with 20 randomly selected single cells. $^{*}p < 0.05$, $^{**}p < 0.01$ as determined using a paired Student *t*-test.

Table 2
Summary table showing the changes in the mechanical properties of HSCs after pre-treating with PBS (control), SDF-1α and H_2O_2 as characterised by AFM and micromanipulation. The Young's modulus, nominal rupture stress and nominal rupture tension significantly decreased with SDF-1α and H_2O_2 pre-treatment when determined from the data corresponding to deformations up to 60% using micromanipulation. However, the Young's modulus significantly increased with SDF-1α and H_2O_2 pre-treatment when cells were tested under smaller deformations using AFM. ↑ and ↓ indicate whether these values increased or decreased compared to PBS pre-treated control cells. Data are presented as the means ± SEM.

Mechanics	Cells			
		PBS-HSCs	SDF-1α-HSCs	H_2O_2-HSCs
AFM	Young's Moduli 10% (Pa)	306.2 ± 15.2	434.9 ± 24.5 ↑	662.8 ± 76.6 ↑
Micromanipulation	Young's Moduli 60% (kPa)	18.1 ± 1.2	13.8 ± 0.8 ↓	14.5 ± 0.8 ↓
	Nominal rupture stress (kPa)	32.70 ± 4.48	17.96 ± 1.77 ↓	23.90 ± 1.51 ↓
	Nominal rupture tension (N/m)	0.23 ± 0.04	0.13 ± 0.02 ↓	0.17 ± 0.02 ↓

from single curves was subsequently converted into 'force versus displacement$^{3/2}$ ' curves, which showed a linear relationship and could be fitted with the Hertz model at deformations less of than 10% (Fig. 4g). The correlation coefficient obtained was 0.99. The Young's modulus values for small deformations were subsequently obtained for pre-treated HSCs. Both SDF-1α ($p < 0.05$) and H_2O_2 ($p < 0.01$) pre-treated cells had significantly higher values that PBS pre-treated cells (Fig. 4h). Moreover, H_2O_2 pre-treatment induced a more significant ($p < 0.05$) change in the Young's modulus value when compared with the effects of SDF-1α. A summary of major HSC findings from micromanipulation and AFM studies can be found in Table 2.

3.7. Pre-treatment of HSCs induced polymerization and reorganisation of F-actin

Flow cytometry demonstrated a significantly increased F-actin accumulation following SDF-1α ($p < 0.05$) and H_2O_2 ($p < 0.05$) pre-treatment when compared to PBS pre-treated cells (Fig. 5a). Furthermore, H_2O_2 induced a more significant ($p < 0.05$) increase in content than SDF-1α. Confocal microscopy of the cell surface revealed that within control cells, the F-actin network was diffuse and distributed evenly within the whole cell. However, with both SDF-1α and H_2O_2 pre-treatment, this staining pattern was disrupted and replaced with more punctate staining potentially indicative of increased F-actin localisation in the outermost cortical region close to the cell membrane (Fig. 5b). Furthermore, the cell membrane appeared more ruffled in appearance compared to the control cells. The level of cellular fluorescence from confocal microscopy images was semi-quantified using ImageJ to obtain a corrected total cell fluorescence (CTCF) value. This showed that pre-treated samples had higher F-actin content which was statistically significant ($p < 0.05$) but only with H_2O_2 pre-treatment (Fig. 5c).

Multiphoton images of treated cells were also acquired from the cell surface and from the mid-region of HSCs in which the nucleus was stained in addition to F-actin (Fig. 6). When imaged at the surface of the cells, the F-actin network within PBS treated control cells was more diffusely distributed within the cell. However, with both SDF-1α and H_2O_2 treatment, this diffuse staining pattern was again disrupted and replaced with multiple clustered regions with significantly increased fluorescent intensity. Larger and more intensely fluorescent clusters were noted with H_2O_2 treatment. When focusing through the cell interior, the nucleus typically occupied most of the space. PBS pre-treated cells again demonstrated uniform F-actin staining on the edges of the cells close to the membrane. However, with SDF-1α and H_2O_2 pre-treatment, clusters with increased fluorescent intensity were again noted.

4. Discussion

Reducing exogenously injected SC entrapment within microvessels of non-specific sites, and thus increasing and maintaining their circulation in peripheral blood, is a potential mechanism for enhancing their homing to sites of injury [13,15,20,21]. Although the larger size of HSCs and particularly MSCs may impact their ability to freely circulate, size does not appear to limit the ability of blood cells to traverse small diameter capillaries. For example, red blood cells have an approximate diameter of 8 µm diameter but can easily circulate through capillaries that are as small as 2–2.5 µm in diameter [41]. Therefore, if SCs possess appropriate deformability, they could avoid pulmonary entrapment, remain circulating and thus increase their chances of active recruitment from flow. Improving SC deformability using pre-treatment strategies or separating SCs based on their mechanical properties may improve their therapeutic efficacy. However, no studies have as yet characterised the mechanical properties of naïve or pre-treated SCs.

An interesting initial observation in this study was the fact both SC types had a size range that was much larger than that of neutrophils. It is not clear why such variations in SC size was observed. However, it is becoming increasingly clear that even SCs isolated from the same site demonstrate heterogeneity with regards their phenotype and function [42,43]. This is particularly true for bone marrow-derived MSCs where at least two sub-populations can be found. When isolated and cultured, clonal expansions showed MSCs possessing either elongated fibroblast-like or flattened and spread phenotypes [43]. This may explain the broad size range for the bone marrow-derived MSCs investigated in the current study. It is also not clear why pre-treated HSCs did not demonstrate any change in cell size, particularly since neutrophils are well known to become larger as a result of activation with inflammatory stimuli [44]. It is possible that HSCs may have required longer than 30 min exposure to SDF-1α /H_2O_2, multiple activators or the presence of physiological blood flow to undergo significant changes in cell size.

This study demonstrated that at large deformations only neutrophils and HSCs underwent rupture, with the force required being similar and both cell types rupturing at ~80% cellular deformation. At first glance, this suggested both neutrophils and HSCs were equally 'strong' or 'stiff'. However, this data did not take into account that the size of these cells was different. Therefore, to make meaningful comparisons between their mechanical strength, nominal rupture stress and tension were calculated, which took into account the different cross-sectional area and diameter of the cells respectively. Once corrected for size, it became apparent that neutrophils were stronger/stiffer cells with HSCs being 'weaker' cells. Since a higher Young's modulus indicates less deformable cells, this value calculated at large deformations also confirmed that

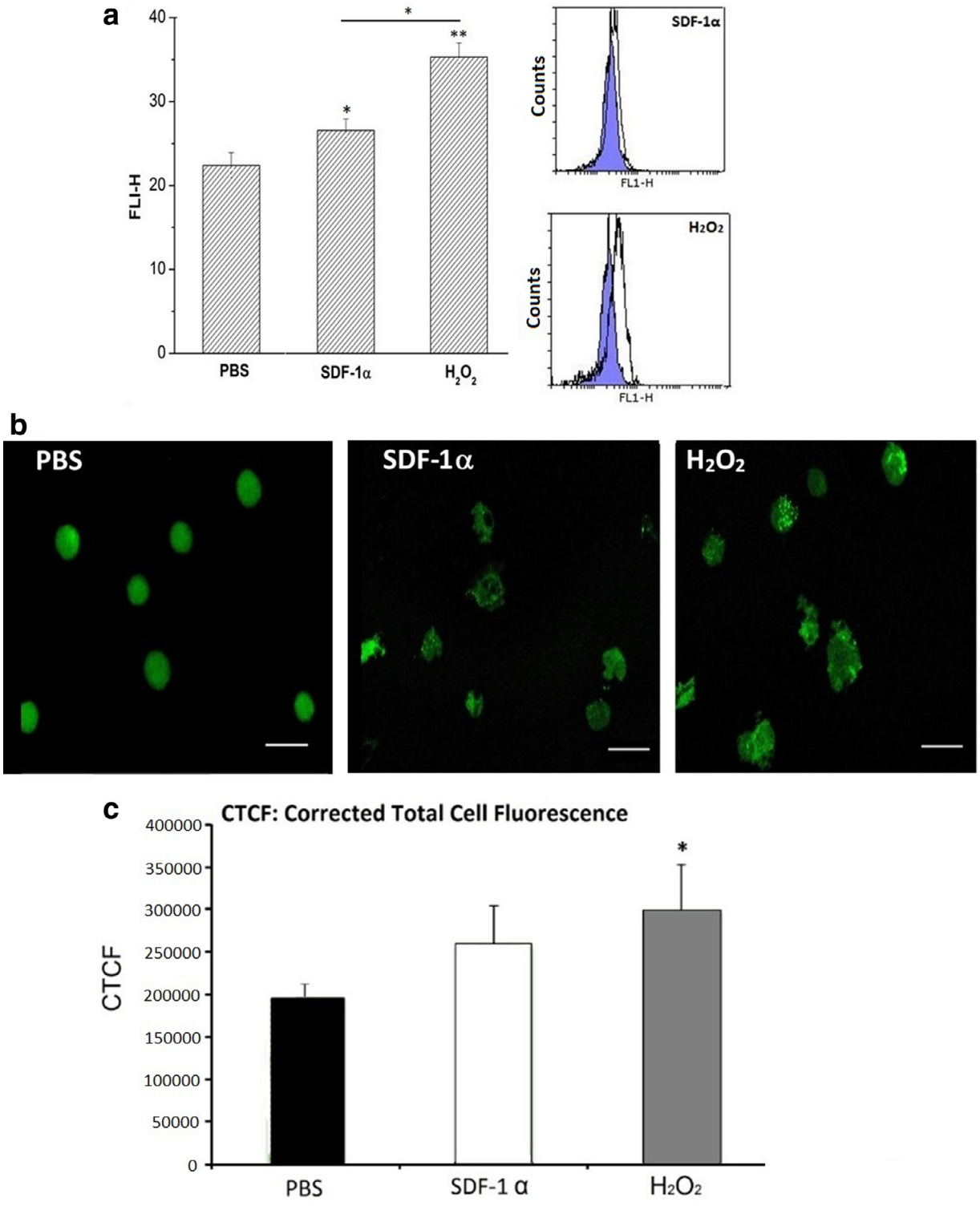

Fig. 5. *Polymerization and reorganization of F-actin after pre-treatment.* **(a)** Mean fluorescence intensity (FLI) for each group as determined using flow cytometry. Cells pre-treated with SDF-1α or H_2O_2 increased F-actin accumulation compared to PBS control group. H_2O_2 induced a more significant change in content than SDF-1α. Typical histograms are shown showing a shift to the right following pre-treatment with SDF-1α and H_2O_2. **(b)** PBS control cells showed more spherical morphologies and smooth surfaces with more diffuse and uniform F-actin staining within the cell cytoplasm. However, within pre-treated HSCs, this uniform staining was replaced with more punctate staining. Only when the focus was on the surface of the cell was punctuate staining observed. When focusing through the cell interior, such F-actin staining was not noted. **(c)** The level of cellular fluorescence from confocal microscopy images was semi-quantified using ImageJ to obtain a corrected total cell fluorescence (CTCF) value. This showed that pre-treated samples had higher F-actin content which was statistically significant but only with H_2O_2 pre-treatment. Scale Bar = 20 μm. $p < 0.05$, $^{**}p < 0.01$ as determined using a paired Student *t*-test. Data are presented as the means±SEM.

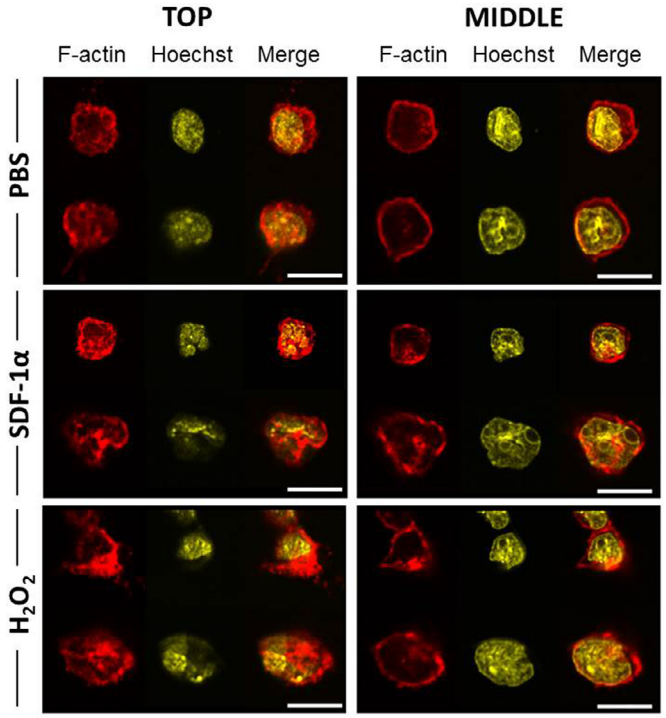

Fig. 6. *Increased presence of F-actin after pre-treatment in outermost cortical regions of treated cells.* Multiphoton microscopy images showing two cells for each group imaged on their surface and at their mid-point. When imaged at the surface, the diffuse F-actin staining noted with PBS treatment is replaced in SDF-1α and H_2O_2 pre-treated cells with multiple clustered regions with significantly increased fluorescent intensity. Larger and more intensely fluorescent clusters were noted with H_2O_2 treatment. When focusing through the cell interior, the nucleus typically occupied most of the space. PBS pre-treated cells again demonstrated uniform F-actin staining on the edges of the cells close to the membrane. However, with SDF-1α and H_2O_2 pre-treatment, clusters with increased fluorescent intensity were again noted. Scale bar = 10 μm.

neutrophils were indeed significantly stiffer than HSCs which were more elastic in nature. A Young's modulus value at large deformation was also determined for MSCs which, interestingly, demonstrated that they were just as deformable as HSCs despite the fact that their overall cell size was much bigger. This novel data is interesting when considering the fact that recruitment of these more deformable SCs is not as rapid or as efficient as the recruitment of the 'stiffer' neutrophil during inflammation [45]. Indeed, we frequently observe intravitally large numbers of neutrophils infiltrating injured tissues within minutes of an inflammatory insult, numbers that far exceed those of recruited HSCs or MSCs. Also, HSC recruitment is much higher than MSCs within a similarly injured tissue [14]. Collectively, this suggests that size is likely to play an important factor in the recruitment of different circulating cell types *in vivo*. Smaller cells such as neutrophils clearly circulate and adhere better than larger SCs cells even though they are a lot stiffer, and therefore deformability may be considered as being of secondary importance.

One of the interesting observations was that during micromanipulation compression, only neutrophils and HSCs demonstrated obvious rupture behaviour, whilst MSCs showed an absence of clear rupture force. These two different mechanical responses are in likely agreement with the two main mechanical behaviour models that have previously been described for cells [46–48]. These models suggest specific structures in a cell dominate its deformability and play a major role in transmitting and distributing mechanical stresses within the cell after exposure to an external force. Cells can behave either more similarly to a 'cortical shell - liquid core' structure or as a 'homogeneous solid state' structure when being compressed by the applied forces. Their response to this stress is suited to the biological processes they need to undergo. The first model assumes that the main cellular structures resisting any external forces are confined within the thin (~100 nm) actin-rich deformable cortex beneath the plasma membrane of the cell [49,50]. In these models, it is assumed that the liquid cell interior or cytoplasm plays little role in resisting mechanical forces. In contrast, some believe the cortical layer does not play a significant role in resisting force and that cells follow the second model which assumes the whole cell is a homogeneous, viscoelastic solid material and that the internal cytoplasmic cytoskeleton is the dominant structure resisting mechanical load. In this model, the contribution of the cortical layer is considered negligible. The 'cortical shell - liquid core' model is widely applied to model suspended cells that are found as spheres in suspension in the body i.e. blood cells. The 'homogenous solid state' model is generally applied to more adherent cells [46–48].

It is still debated whether cells behave more similarly to a 'cortical shell - liquid core' or to a 'homogeneous solid state' structure. However, since we demonstrated two clearly different rupture characteristics, it is possible that the tested SCs follow one or the other of these two models. These mechanical properties likely mirror the in vivo functional distinctions of these cell types. Although HSCs are adherent within the BM, they can exit it following remote injury and travel via the circulation, similarly to blood neutrophils, to sites of injury. Hence both these cell types probably follow the 'cortical shell - liquid core' model applied to spherical cells found in suspension. The clear rupture force of neutrophils and HSCs, therefore may have resulted from the breakage of their cortical shell. The subsequent compression of the liquid interior after shell rupture induced the rapid measured decrease in the force in the force-displacement curves. In contrast to suspended cells, MSCs are primarily classed as adherent cells that adhere to each other or to their substrate throughout their lifetime and do not generally exit their niche and circulate in peripheral blood under physiological conditions. Hence for MSCs, which are not designed to be circulating cells, the 'homogenous solid state' model may be more relevant [46]. The homogenous, viscous nature of the whole cell most likely explained their ability to withstand force and therefore not undergo rupture. Indeed, in culture MSCs can readily assume a flattened appearance.

Micromanipulation and AFM studies were also conducted on HSCs pre-treated with well known inflammatory factors, namely SDF-1α and H_2O_2. These non-genetically modified approaches to increase SC homing and recruitment provide the potential for them to be used clinically as an adjuvant therapy to enhance SC effectiveness. Since a lower Young's modulus indicates more deformable cells, the data obtained at large deformations of 60% demonstrated that both pre-treatments generated HSCs which were significantly more deformable than PBS pre-treated cells. Similarly, the nominal rupture stress/tension of these pre-treated HSCs also decreased. This collectively suggested the cells as a whole became weaker and more deformable after pre-treatment. This 'softening' after pre-treatment is in accordance with our previously published work using a more basic micropipette aspiration method [21]. White and colleagues showed that when 10 μm HSCs were sucked into 5 μm micropipettes, and thus squeezed to large deformations, the time it took to fully aspirate them was reduced following SDF-1α pre-treatment [21]. These pre-treatment strategies have multiple beneficial effects. Their ability to improve SC deformability could enhance and maintain their presence within the circulation, but they also modify the clustering of HSC surface integrins and increase their affinity for endothelial counterligands which improves their retention within injured tissue microvessels [30,31].

In contrast to the micromanipulation data, the Young's modulus calculated following small deformations using AFM increased with similar pre-treatments, particularly H_2O_2, which suggested that the HSC surface that was being probed had stiffened. This stiffening of the cell surface after pre-treatment can potentially be explained by the expansion and polymerization of F-actin to the plasma membrane. Indeed, the increased immunostaining of F-actin filaments noted in the cortical membrane confocally after pre-treatment may allow for the observed increase in the cell surface elasticity modulus at small deformations. Multiphoton images appeared to confirm the possibility that the presence of F-actin increased in clustered regions in the outer cortical region close to the cell membrane. It is well established that one of the earliest effects (within 1 min) of inflammatory mediators on neutrophils is to cause them to become stiffer and less deformable. Most often these effects are short-lived and disappear after $\sim$30 min [49]. This enhanced stiffness is thought to be due to the polymerisation of G-actin to F-actin that forms a sub-cortical shell beneath the membrane. Actin is a key component of the neutrophil cytoskeleton and contributes to the cell stiffness. Polymerization from a globular monomeric G-actin form to a filamentous F-actin form leads to neutrophil stiffening. This increased stiffness enhances the margination of neutrophils in inflamed regions and delays their transit which encourages binding through integrin activation. On the downside, this increased stiffening can lead to neutrophil sequestration within the pulmonary microvessels. F-actin observations made in the current study in HSCs after pre-treatment with SDF-1α and H_2O_2 suggested that overall F-actin content was increased and F-actin appeared restructured from uniform to more punctate and *clustered* staining. Although overall content was increased, it appeared increased primarily in the outermost cortical region close to the cell membrane. This would suggest that pre-treated HSCs were stiffer in their cortical region due to the increased F-actin beneath the plasma membrane, an observation that is similarly observed in neutrophils. However, these preliminary finding would require further detailed investigation with more accurate cytoskeletal staining and powerful imaging modalities such as super-resolution or total internal reflection fluorescence (TIRF) microscopy.

The mechanical property parameters derived in this study may not be able to perfectly reflect the inherent architectural structure of the actin network within these specific cells. Nevertheless, the calculations of Young's modulus derived from the data can still be used to evaluate the stiffness of individual cells. Due to the complex contributions of various cellular components (actin, nucleus, cytoskeleton etc.) in response to different applied load, more complex mathematical modelling methods such as finite element analysis (FEA) would be an ideal approach to completely quantify the data. FEA is a computerized method for predicting how different components within cells would specifically react to physical forces applied to them. While FEA may offer the means to predict how the different cellular components may react to physical forces, this is beyond the scope of the present study.

5. Conclusions

Improving the retention efficiency of circulating SCs within sites of injury may depend on manipulating their mechanical properties or isolating smaller and more deformable sub-populations for infusion. Prior to conducting such strategies, some information on the mechanical properties of different therapeutic cells was required. Novel micromanipulation and AFM studies on HSCs and MSCs demonstrated that surprising mechanical distinctions exist amongst different therapeutic cells with regards their deformability and also their rupture response to applied stress. Although distinct differences were observed between these two SC populations, this study also suggests intra-population variation exists within naïve and pre-treated HSCs. The mechanical properties of individual HSCs are force/deformation-dependent and highly non-linear from the cell surface to the internal cytoskeleton regarding the structure and concentration of actin filaments. These different mechanical parameters particularly the variations in the deformability, can potentially be utilized as label-free markers in microfluidic cell sorting systems to separate different sub-populations of potentially more therapeutic SCs.

Declaration of Competing Interest

None declared.

Funding

MMD was financially supported by a Li Siguang Scholarship from the University of Birmingham, UK and a scholarship from China Scholarship Council, both of which are much appreciated.

Ethical approval

Not required.

References

[1] Dimmeler S, Burchfield J, Zeiher AM. Cell-based therapy of myocardial infarction. Arterioscler Thromb Vasc Biol 2008;28:208–16.
[2] Volkman R, Offen D. Concise review: mesenchymal stem cells in neurodegenerative diseases. Stem Cells 2017;35:1867–80.
[3] Mahmood A, Lu D, Wang L, et al. Treatment of traumatic brain injury in female rats with intravenous administration of bone marrow stromal cells. Neurosurgery 2001;49:1196–204.
[4] Ukai R, Honmou O, Harada K, et al. Mesenchymal stem cells derived from peripheral blood protects against ischemia. J. Neurotrauma 2007;24:508–20.
[5] Salem GA, Selby GB. Stem cell transplant in inflammatory bowel disease: a promising modality of treatment for a complicated disease course. Stem Cell Investig 2017;29(4):95.
[6] Houlihan DD, Newsome PN. Critical review of clinical trials of bone marrow stem cells in liver disease. Gastroenterology 2008;135:438–50.
[7] Lehmann G, Palmero P, Cacciotti I, et al. Design, production and biocompatibility of nanostructured porous HAp and Si-hap ceramics as three-dimensional scaffolds for stem cell culture and differentiation. Ceram Silik 2010;54:90–6.
[8] Bianco A, Bozzo BM, Del Gaudio C, et al. Poly(L-lactic acid)/calcium-deficient nanohydroxyapatite electrospun mats for murine bone marrow stem cell cultures. J Bioact Compat Polym 2011;26:225–41.
[9] D'Angelo F, Armentano I, Cacciotti I, et al. Tuning multi-/pluri-potent stem cell fate by electrospun poly(L-lactic acid)-calcium-deficient hydroxyapatite nanocomposite mats. Biomacromolecules 2012;13:1350–60.
[10] Cacciotti I, Ciocci M, Di Giovanni E, et al. Hydrogen sulfide-releasing fibrous membranes: potential patches for stimulating the human stem cells proliferation and viability under oxidative stress. Int J Mol Sci 2018;19:E2368.
[11] Cacciotti I, Ceci C, Bianco A, et al. Neuro-differentiated Ntera2 cancer stem cells encapsulated in alginate beads: first evidence of biological functionality. Mater Sci Eng 2017;81:32–8.
[12] Ciocci M, Cacciotti I, Seliktar D, et al. Injectable silk fibroin-hydrogels functionalized with microspheres as adult stem cells-carrier systems. Int J Bio Macromol 2018;108:960–71.
[13] Karp JM, Teo GS. Mesenchymal stem cell homing: the devil is in the details. Cell Stem Cell 2009;4:206–16.
[14] Kavanagh DP, Suresh S, Newsome PN, et al. Pretreatment of mesenchymal stem cells manipulates their vasculoprotective potential while not altering their homing within the injured gut. Stem Cells 2015;33:2785–97.
[15] Fischer UM, Harting MT, Jimenez F, et al. Pulmonary passage is a major obstacle for intravenous stem cell delivery: the pulmonary first-pass effect. Stem Cells Dev 2009;18:683–92.
[16] Toma C, Wagner WR, Bowry S, et al. Fate of culture-expanded mesenchymal stem cells in the microvasculature: in vivo observations of cell kinetics. Circ Res 2009;104:398–402.
[17] Doerschuk CM, Beyers N, Coxson H, et al. Comparison of neutrophil and capillary diameters and their relation to neutrophil sequestration in the lung. J Appl Physiol 1993;74:3040–5.
[18] Tse W, Nash GB, Hewins P, et al. ANCA-induced neutrophil F-actin polymerization: implications for microvascular inflammation. Kidney Int. 2005;67:130–9.
[19] Yap B, Kamm RD. Mechanical deformation of neutrophils into narrow channels induces pseudopod projection and changes in biomechanical properties. J Appl Physiol 2005;98:1930–9.
[20] Lipowsky HH, Bowers DT, Banik BL, et al. Mesenchymal stem cell deformability and implications for microvascular sequestration. Ann Biomed Eng 2018;46:640–54.

[21] White RL, Nash G, Kavanagh DP, et al. Modulating the adhesion of haematopoietic stem cells with chemokines to enhance their recruitment to the ischaemically injured murine kidney. PLoS ONE 2013;8:e66489.
[22] Guck J, Schinkinger S, Lincoln B, et al. Optical deformability as an inherent cell marker for testing malignant transformation and metastatic competence. Biophys J 2005;88:3689–98.
[23] Fritsch A, Höckel M, Kiessling T, et al. Are biomechanical changes necessary for tumour progression? Nat Phys 2010;6:730–2.
[24] Meinhövel F, Stange R, Schnauss J, et al. Changing cell mechanics - a precondition for malignant transformation of oral squamous carcinoma cells. Converg Sci Phys Oncol 2018;4:034001.
[25] Gossett DR, Weaver WM, Mach AJ, et al. Label-free cell separation and sorting in microfluidic systems. Anal Bioanal Chem 2010;397:3249–67.
[26] Mcfaul SM, Lin BK, Ma H. Cell separation based on size and deformability using microfluidic funnel ratchets. Lab Chip 2012;12:2369–76.
[27] Zemla J, Danilkiewicz J, Orzechowska B, et al. Atomic force microscopy as a tool for assessing the cellular elasticity and adhesiveness to identify cancer cells and tissues. Semin Cell Dev Biol 2018;73:115–24.
[28] Pinto do Ó, Kolterud PA, Carlsson L. Expression of the LIM-homeobox gene LH2 generates immortalized steel factor-dependent multipotent hematopoietic precursors. EMBO J 1998;17:5744–56.
[29] Pinto do Ó, Richter PK, Carlsson L. Hematopoietic progenitor/stem cells immortalized by Lhx2 generate functional hematopoietic cells in vivo. Blood 2002;99:3939–46.
[30] Kavanagh DP, Yemm AI, Alexander JS. Enhancing the adhesion of hematopoietic precursor cell integrins with hydrogen peroxide increases recruitment within murine gut. Cell Transplant 2013;22:1485–99.
[31] Kavanagh DP, Yemm AI, Zhao Y, et al. Mechanisms of adhesion and subsequent actions of a haematopoietic stem cell line, HPC-7, in the injured murine intestinal microcirculation in vivo. PLoS ONE 2013;8:e59150.
[32] Kavanagh DP, Durant LE, Crosby HA, et al. Haematopoietic stem cell recruitment to injured murine liver sinusoids depends on $\alpha 4\beta 1$ integrin/VCAM-1 interactions. Gut 2010;59:79–87.
[33] Houlihan DD, Mabuchi Y, Morikawa S, et al. Isolation of mouse mesenchymal stem cells on the basis of expression of Sca-1 and PDGFR-α. Nat Protoc 2012;7:2103–11.
[34] Nauseef WM. Isolation of human neutrophils from venous blood. Neutrophil methods and protocols Methods in molecular biology™, 412. Humana Press; 2007.
[35] Du M, Kalia N, Frumento G. Biomechanical properties of human t cells in the process of activation based on diametric compression by micromanipulation. Med Eng Phys 2017;40:20–7.
[36] Nguyen BV, Wang QG, Kuiper NJ, et al. Biomechanical properties of single chondrocytes and chondrons determined by micromanipulation and finite-element modelling. J R Soc Interface 2010;7:1723–33.
[37] Kuznetsova TG, Starodubtseva MN, Yegorenkov NI, et al. Atomic force microscopy probing of cell elasticity. Micron 2007;38:824–33.
[38] Martens JC, Radmacher M. Softening of the actin cytoskeleton by inhibition of myosin II. Pflügers Arch Eur J Physiol 2008;456:95–100.
[39] Yan Y, Zhang Z, Stokes JR, et al. Mechanical characterization of agarose micro–particles with a narrow size distribution. Powder Technol 2009;192:122–30.
[40] Note J.A. Determining the elastic modulus of biological samples using the atomic force microscope. https://www.jpk.com/app-technotes-img/AFM/pdf/jpk-app-elastic-modulus.14-1.pdf.
[41] Kwan JM, Guo Q, Kyluik-Price DL, et al. Microfluidic analysis of cellular deformability of normal and oxidatively damaged red blood cells. Am J Hematol 2013;88:682–9.
[42] Rennerfeldt DA, Van Vliet KJ. Concise Review: when colonies are not clones: evidence and implications of intracolony heterogeneity in mesenchymal stem cells. Stem Cells 2016;34:1135–41.
[43] James S, Fox J, Afsari F, et al. Multiparameter analysis of human bone marrow stromal cells identifies distinct immunomodulatory and differentiation-competent subtypes. Stem Cell Rep 2015;4:1004–15.
[44] Ekpenyong AE, Toepfner N, Chilvers ER, et al. Mechanotransduction in neutrophil activation and deactivation. Biochim Biophys Acta 2015;1853:3105–16.
[45] Summers C, Rankin SM, Condliffe AM, et al. Neutrophil kinetics in health and disease. Trends Immunol. 2010;31:318–24.
[46] Stamenović D, Ingber DE. Models of cytoskeletal mechanics of adherent cells. Biomech Model Mechanobiol 2002;1:95–108.
[47] Lim C, Zhou E, Quek S. Mechanical models for living cells - a review. J Biomech 2006;39:195–216.
[48] Bansod YD, Bursa J. Continuum-based modelling approaches for cell mechanics. World Acad Sci Eng Technol Int J Biol Biomol Agric Food Biotechnol Eng 2015;9:921–32.
[49] Saito H, Lai J, Rogers R, et al. Mechanical properties of rat bone marrow and circulating neutrophils and their responses to inflammatory mediators. Blood 2002;99:2207–13.
[50] Liu F, Wu D, Chen K. A zebrafish embryo behaves both as a “cortical shell–liquid core” structure and a homogeneous solid when experiencing mechanical forces. Microsc Microanal 2014;20:1841–7.